# MgAPSO-34 molecular sieves with various Mg stoichiometries: Synthesis, characterization and catalytic behavior in the direct transformation of chloromethane into light olefins

Dazhi Zhang [a], Yingxu Wei [a], Lei Xu [a], Fuxiang Chang [a], Ziyu Liu [a], Shuanghe Meng [a], Bao-Lian Su [a,b,*], Zhongmin Liu [a*]

[a] Applied Catalysis Laboratory, Dalian Institute of Chemical Physics, Chinese Academy of Sciences, 457 Zhongshan Road, P.O. Box 110, Dalian 116023, China
[b] Laboratory of Inorganic Materials Chemistry, The University of Namur (FUNDP), 61 Rue de Bruxelles, B-5000 Namur, Belgium

## ARTICLE INFO

## ABSTRACT

A series of MgAPSO-34s with various Mg stoichiometries were synthesized, characterized by multiple techniques such as, powder XRD, solid state MAS NMR, DR UV–vis spectrometry, $NH_3$-TPD and FTIR and used as catalysts in the direct conversion of chloromethane into light olefins. XRD results revealed that the unit cell parameters of the CHA structure increased with Mg incorporation. The appearance of some new peaks in the $^{31}P$ MAS NMR spectra of MgAPSO-34 indicated new P co-ordination states as a result of the substitution of Al by Mg. Mg incorporation also modified the Si co-ordination states. A DR UV–vis spectroscopic study evidenced that, in comparison with an MgO crystal, the Mg species in the MgAPSO-34s were quite different. These changes in crystal structure and the chemical environment of framework elements created by Mg substitution modified the acidity and catalytic properties. The acidity of SAPO-34 and MgAPSO-34 determined with $NH_3$-TPD and FTIR techniques showed that the amount of acid sites, especially those of strong acidity, is reduced with the increase of Mg incorporation. Direct chloromethane transformation was carried out over SAPO-34 and MgAPSO-34. All the samples were very active and selective catalysts for light olefin production from chloromethane. Compared with SAPO-34, MgAPSO-34 showed an enhanced conversion, longer catalyst life and improved light olefin selectivity.

© 2008 Elsevier Inc. All rights reserved.

## 1. Introduction

Aluminophosphate (AlPOs) and silicoaluminophosphate (SAPOs) molecular sieves, microporous materials with P-Al or Si-P-Al frameworks, have been widely used as shape-selective catalysts in many processes [1–3]. Among SAPO molecular sieves, small pore SAPO-34 exhibited particularly high ethylene and propylene selectivity in the MTO process [4]. Many elements have been incorporated into the SAPO-34 framework by isomorphous substitution to form MeAPSO molecular sieves (Me = Be, B, Mg, Ti, Mn, Fe, Co, Ni, etc.) [5,6]. With this modification, MeAPSO-34 showed improved light olefin selectivity. For instance, Ni incorporation gave rise to extremely high ethylene selectivity up to 90% and using SrAPSO-34, ethylene and propylene selectivity attained 89.5% [7,8].

Although the difference in catalytic performance between SAPOs and MeAPSOs have been presented in the literature, theoretical and experimental details about the effect of metal incorporation on co-ordination state of other framework elements, such as Al, P and Si, is sparse [2,3]. In the case of MgAPSO molecular sieves, metal ions are substituted on to the $Al^{3+}$ site within the framework which generates P(nAl, (4−n)Mg) co-ordination environments [9–12]. The work of Ashtekar et al. and our recent study indicated that metal incorporation into SAPO frameworks gave rise to more silicon-rich regions [12]. Akporiaye et al. proposed that in the MgAPSOs, the only likely site for silicon incorporation was the P(4Al) site [13]. These observations predicted the differences between acidity and catalytic properties of MeAPSO and SAPO molecular sieves, whereas the correlation between metal incorporation and catalytic property improvement is still elusive. The clarification of the influence caused by metal incorporation and the corresponding change in catalytic performance merit a more detailed investigation.

In this present work, a series of MgAPSO-34s were synthesized using triethylamine as a template. The co-ordination states and variation in acidity upon incorporation of differing amounts of Mg within the framework were compared. A previous study proved

that SAPO-34 and MeAPSO-34 are excellent catalysts for the production of light olefins from methanol [14,15]. Our recent work has indicated that SAPO-34 and MnAPSO-34, aside from their successful application in the MTO process, are potential catalysts in the direct transformation of chloromethane into light olefins, which is regarded as an alternative use of natural gas with halogenated methane as an intermediate [16–22].

This process was first proposed by Olah et al. [23] and zeolites, such as ZSM-5, Y and MOR, were usually employed as catalysts for the transformation of halogenated methane into higher hydrocarbons [24–32]. Products suitable for gasoline were mainly produced over zeolite catalysts. However, their performance for light olefin production needed further improvement. Mild acidity and the small pore openings of SAPO-34 made it possible for highly efficient chloromethane conversion and a high selectivity for light olefins. In the present work, besides the study of metal incorporation, we also try to develop a new SAPO-34 catalyst by modifying the Mg content to improve the performance of chloromethane transformation into light olefins.

# 2. Experimental

## 2.1. Synthesis

SAPO-34 and MgAPSO-34s were hydrothermally synthesized according to a reported method [33]. The starting gels, with chemical composition of $1.0Al_2O_3:1.0P_2O_5:0.6SiO_2:xMgO:3NEt_3:50H_2O$ ($x = 0 – 0.20$) were prepared by mixing pseudoboehmite (PetroChina, China), orthophosphoric acid (85 wt.%, LiaoningChem, China), silica sol (25 wt.%, ShanghaiChem, China) and deionized water with vigorous stirring, and then followed by addition of the template (Triethylamine, TEA, XinxiChem, China) and magnesium acetate (ShanghaiChem, China) solution. The gels were sealed in the autoclaves and crystallized at 200 °C for 15 h under autogenous pressure. The crystals were filtered, washed with deionized water, dried at 120 °C for 12 h, and then calcined in air at 550 °C for 4 h to remove the template. The obtained samples with $x = 0$, 0.05, 0.10, 0.15, 0.20 were denoted as Mg34-00, Mg34-05, Mg34-10, Mg34-15 and Mg34-20.

## 2.2. Characterization

Chemical composition was determined with a Philips Magix X-Ray Fluorescence spectrometer. The powder XRD patterns were recorded on a D/MAX-b X-ray diffractometer with CuKα1 radiation ($\lambda = 1.5406$ Å). Morphology of all the samples was obtained on a kyky 1000 scanning electron microscope. Diffuse reflectance UV–vis spectra of the calcined samples were recorded using a JASCO V-550 UV–vis spectrophotometer. Solid-state $^{27}$Al, $^{31}$P and $^{29}$Si MAS NMR spectra were obtained on a Varian Infinity-Plus 400 NMR spectrometer with a BBO MAS probe. Solid-state $^{27}$Al, $^{31}$P and $^{29}$Si MAS NMR spectra were obtained on a Varian Infinity-Plus 400 MHz NMR spectrometer. $^{27}$Al MAS NMR experiments were carried out using a 4 mm MAS NMR probe with a spinning rate of 10 kHz. Chemical shifts were referenced to 1 $Al(H_2O)_3^{6+}$. $^{31}$P MAS NMR spectra were measured at 161.90 MHz on a 4 mm probe spinning at 10 kHz. $^{29}$Si MAS NMR spectra with high power proton decoupling were recorded at 79.4 kHz using a 7.5 mm MAS probe with a spinning rate of 4 kHz. 4,4-dimethyl-4-silapentane sulfonate sodium (DSS) was used as the chemical shift reference for $^{29}$Si MAS NMR spectroscopy.

The NH$_3$-TPD experiment was performed with a Micromeritics Autowin 2910 Chemical adsorption apparatus. 0.15 g calcined samples (40 – 60 mesh) were first activated at 650 °C for 30 min under a He flow of 20 ml/min. NH$_3$ was injected to saturate the samples at 100 °C. NH$_3$ desorption was measured from 100 °C to 650 °C at a constant heating rate of 10 °C/min in a He flow of 40 ml/min.

The in situ FT-IR measurements were used to determine the acidity of the catalyst with ammonia as the probe molecule. A 10 mg catalyst sample was pressed into a self-supported wafer with a diameter of 13 mm. The wafer was placed in a quartz cell equipped with CaF$_2$ windows and treated in a vacuum ($10^{-2}$ Pa) at 500 °C for 2 h. After cooling to room temperature, a spectrum was recorded using a Fourier Transform Infrared Spectrometer (Bruker Equinox 55). Ammonia adsorption was then conducted on the wafer at 100 °C and a spectrum of the solid phase was recorded after removing the gas phase ammonia by evacuation.

## 2.3. Catalytic test

Chloromethane transformation was carried out in a fixed-bed quartz reactor at atmospheric pressure. 0.62 g catalyst (40–60 mesh) was loaded into the reactor and 3 ml quartz chips in the upper part of the reactor were used to preheat the reactant gas. All the samples were evaluated at 450 °C. Before each test, the catalyst was treated in flowing N$_2$ at reaction temperature for 1 h. Then the CH$_3$Cl flow (WHSV = 3.2 h$^{-1}$) diluted by N$_2$ (CH$_3$Cl: N$_2$ = 1:1) was introduced. All the products from the outlet of the reactor were kept at 150 °C and analyzed by an on-line Varian 3800 gas chromatograph equipped with a FID detector and a Pona capillary column (50 m).

# 3. Results and discussion

## 3.1. Synthesis

### 3.1.1. Chemical composition

The bulk chemical compositions of the synthesized SAPO-34 and MgAPSO-34 are given in Table 1. Among the five samples, Mg34-00 shows the highest Si content (5.02 wt.%). Upon Mg incorporation, the fraction of Si in the as-synthesized samples decreases. This is most noticeable when the Mg content reaches 1.65 wt.% with just 3.16 wt.% Si present in the Mg34-20 crystal. For a clear comparison of element substitution within a framework, the synthesis of SAPO-34 and MgAPSO-34 was performed from the starting gel with the same Al:P:Si ratio and the same template, only the Mg content of the gel varied. The chemical composition of the synthesized samples indicates that the presence of Mg in the starting gel has an effect on the Si substitution into the molecular sieve frameworks.

### 3.1.2. Crystalline structure and morphological features by powder XRD and SEM

The powder X-ray diffraction patterns of the as-synthesized and calcined SAPO-34 and MgAPSO-34 molecular sieves are shown in Fig. 1. All the diffraction lines in the patterns can be indexed using a typical zeolite CHA crystalline structure [2]. Mg incorporation into the framework (Fig. 1A(b–e)) gives rise to some new peaks at $2\theta = 17.6$, 24.7, 33.1, 34.8, 35.6, 36.2 and 42.9°, compared to the pattern of SAPO-34 (Fig. 1A(a)), indicating a change in symmetry. Most of the peaks in the patterns of MgAPSO-34 appear with higher intensity than those of SAPO-34, suggesting a more crystalline structure. The crystallographic data listed in Table 1 also proves the higher crystallinity of Mg incorporated samples. After calcination, SAPO-34 and MgAPSO-34 retain the zeolite CHA structure and the diffraction line at 9.4° ($2\theta$) becomes very strong in all the patterns.

Another interesting observation is that, compared with SAPO-34, the XRD diffraction peaks of MgAPSO-34 shift to lower angles,

**Table 1**
Chemical composition crystallinity and unit cell parameters of the as-synthsized SAPO-34 and MgAPSO-34s

| Sample | Chemical composition (mol) | Mg content (wt.%) | Si content (wt.%) | Crystallinity [a] | Unit cell parameters | | | |
|--------|---------------------------|-------------------|-------------------|-------------------|---------------------|--------|----------|-------|
| | | | | | $a = b$ (Å) | $c$ (Å) | $V$ (Å$^3$) | SD |
| Mg34-00 | $Al_{0.488}P_{0.404}Si_{0.106}O_2$ | 0.00 | 5.02 | 100 | 13.804 | 14.922 | 2462.5 | 0.023 |
| Mg34-05 | $Mg_{0.013}Al_{0.465}P_{0.425}Si_{0.098}O_2$ | 0.33 | 4.51 | 116 | 13.821 | 14.932 | 2470.0 | 0.017 |
| Mg34-10 | $Mg_{0.014}Al_{0.464}P_{0.427}Si_{0.096}O_2$ | 0.35 | 4.46 | 129 | 13.874 | 15.031 | 2505.7 | 0.053 |
| Mg34-15 | $Mg_{0.032}Al_{0.450}P_{0.434}Si_{0.085}O_2$ | 0.83 | 3.91 | 128 | 13.881 | 15.084 | 2517.1 | 0.041 |
| Mg34-20 | $Mg_{0.064}Al_{0.425}P_{0.443}Si_{0.068}O_2$ | 1.65 | 3.16 | 136 | 13.890 | 15.174 | 2535.4 | 0.045 |

[a] Crystallinity calculation based on the peaks of $2\theta$ = 9.45, 12.81, 15.96, 20.51, 25.78 and 30.50°, the crystallinity of MG-00 was set as 100%.
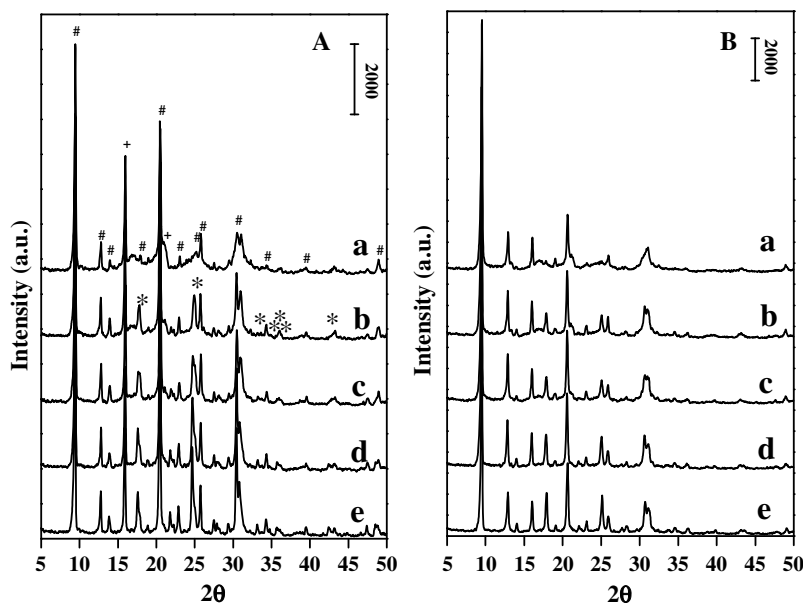


**Fig. 1.** XRD patterns of as-synthesized (A) and calcined (B) samples. (a) Mg34-00, (b) Mg34-05, (c) Mg34-10, (d) Mg34-15 and (e) Mg34-20. (*New peaks after Mg incorporation, #intensity increased, +intensity decreased.)

which implies an increase in the interplanar spacing and thus the lattice parameters as a result of Mg incorporation. This increase may stem from a longer Mg–O bond distance in comparison with the Al–O bond distance [9]. The unit cell parameters of SAPO-34 and MgAPSO-34 are determined by a R3m symmetry in a hexagonal system and the results are listed in Table 1. As the larger $Mg^{2+}$ ion is incorporated into the framework the unit cell parameters increase. Such increases, observed experimentally, provide evidence that Mg incorporation has taken place.

The SEM photos of the as-synthesized SAPO-34 and MgAPSO-34 are depicted in Fig. 2. The crystals show cubic morphology and some twinned crystals can be observed. SAPO-34 particles are uniform, with a size of 1 μm (Fig. 2a), while MgAPSO-34 particles range from 1 to 20 μm (Fig. 2b–e). Some larger particles are generated with Mg incorporation. The crystal size increases with Mg content for the MgAPSO-34 samples.

## 3.2. Chemical environments by $^{27}Al$, $^{31}P$ and $^{29}Si$ MAS NMR and diffuse reflectance UV–vis spectroscopy

### 3.2.1. $^{27}Al$, $^{31}P$ and $^{29}Si$ MAS NMR spectra

The $^{27}Al$ MAS NMR spectra of the as-synthesized SAPO-34 and MgAPSO-34 are given in Fig. 3. All these spectra show a strong signal with a chemical shift of 37.4 ppm, which is the typical signal of Al in a tetrahedral environment Al(4P) for SAPO type molecular sieves. The other signal with lower intensity at 7.9–12.9 ppm is attributed to the penta-coordinated Al from an additional co-ordi-

nation of framework Al atoms with $H_2O$ or template molecules in the channels [34].

The $^{31}P$ MAS NMR spectra of the as-synthesized SAPO-34 and MgAPSO-34 are shown in Fig. 4. For SAPO-34 (Fig. 4a), only one strong signal with a chemical shift of −28.4 ppm is observed, indicative of one chemical environment for P, P(4Al), within the framework [33]. With Mg incorporation, besides the strong signal at −28.4 ppm, three signals with chemical shifts of −25.0, −22.0 and −17.0 ppm progressively appear with relatively low intensity (Fig. 4b and c). With further Mg incorporation, an additional but very low intensity signal at −11.9 ppm is also observed (Fig. 4d and e). The two overlapped signals at −25.0 and −22.0 ppm were attributed to two different P(3Al, 1Mg) units in MgAPSO-34 [11,12]. The weak signals at −17.0 and −11.9 ppm were assigned to P(2Al, 2Mg) and P(1Al, 3Mg) species, respectively. The various chemical environments observed for P, such as P(3Al, 1Mg), P(2Al, 2Mg) and P(1Al, 3Mg), directly prove the occurrence of isomorphous substitution of Mg for framework Al.

A detailed analysis of the chemical environment of phosphorus in MgAPSO-34, by the deconvolution of $^{31}P$ NMR spectra using a Gaussian form are given in Fig. 4 and Table 2. The general trend is that greater P incorporation generates more P(3Al, 1Mg), P(2Al, 2Mg) and P(1Al, 3Mg) species, and conversely less P(4Al) species. It is observed that P(3Al, 1Mg) and P(2Al, 2Mg) species appear when Mg is first introduced into the framework. The P(1Al, 3Mg) species appear only when relatively high stoichiometries of framework Mg are attained (Mg34-15).
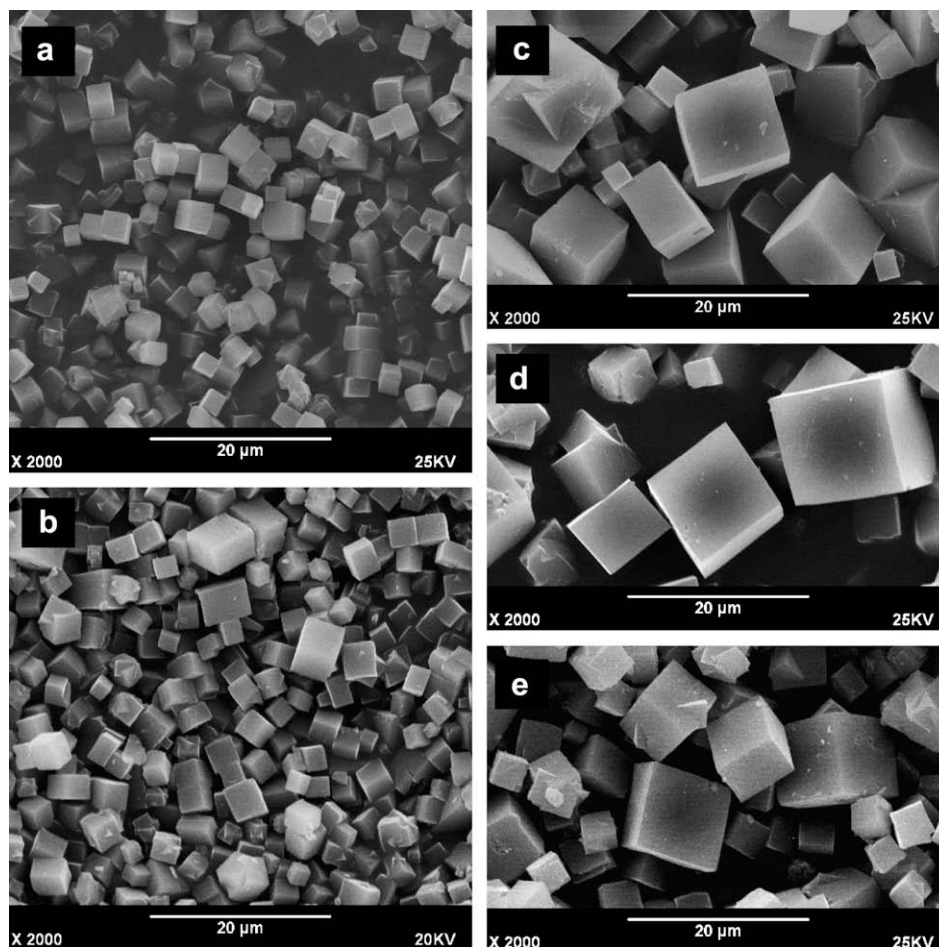
Fig. 2. Scanning electron micrographs of as-synthesized samples. (a) Mg34-00, (b) Mg34-05, (c) Mg34-10, (d) Mg34-15 and (e) Mg34-20.

The ^{29}Si MAS NMR spectra of the as-synthesized SAPO-34 and MgAPSO-34 are shown in Fig. 5. All the spectra show a strong signal with a chemical shift of −91.4 ppm and three signals with low intensity at −95.2, −100.0 and −109.5 ppm. Compared with SAPO-34, no additional signal is observed in the spectra of MgAPSO-34, indicating that no new Si species are generated with Mg incorporation. This is in agreement with the published results that the substitution of Si for the P atom connected to one or more Mg atoms is the most prohibited and the Si–O–Mg bond cannot form [12,13]. For the four signals present in the spectra, the signal at −91.3 ppm is assigned to a Si(4Al) species, generated from one Si substituting for one P by a SM2 mechanism, while the other three peaks at −95.2, −100 and −109.6 ppm are assigned to Si(3Al), Si(2Al) and Si(0Al) species, respectively, stemming from Si incorporation into the framework by the routes of SM3 and SM2 [35].

Although, these four signals appear in all the ^{29}Si MAS NMR spectra, their intensities vary with the stoichiometry of Mg Fig. 5 gives the deconvolution results by Gaussian form and the detailed Si chemical environments within the framework are presented in Fig. 6. Compared with Mg34-00, Mg34-05 containing a low amount of Mg yields a slight increase in Si(4Al) species. As the stoichiometry of Mg increases, the amount of Si(4Al) species decreases. For all the MgAPSO-34 samples, the amount of Si(3Al) and Si(2Al) species is less than in SAPO-34, while the amount of Si(0Al) species becomes more significant in the framework of Mg34-15 and Mg34-20. It is well-known that an increase in Si-island formation within a SAPO framework is usually accompanied by the incorporation of more Si [35]. In the present study, more silica-islands form in the

MgAPSO-34 framework with high Mg content, despite only a small amount of Si. Both Mg incorporation and Si incorporation therefore influence the silicon chemical environment. In the sample with low Mg content, such as Mg34-05, the incorporation of Mg causes the decrease in silica within the framework. Also the Si(4Al) species is more predominant. With the increase of Mg content, more silica-islands are formed as a result of substitution limitation of Si for P, caused by the generation of P(nAl, (4−n)Mg).

Si incorporation into an AlPO framework generates bridge hydroxyl groups used as reaction centers in acid-catalyzed reactions. The acidity strength varies with the Si chemical environment [36]. In the present study, the presence of Mg in the framework inhibits Si incorporation and changes the Si distribution within the framework, so the generated acid sites and their acid properties are modified correspondingly.

### 3.2.2. UV–vis diffuse reflectance spectra

The diffuse reflectance UV–vis spectra of the as-synthesized and calcined samples are given in Fig. 7. These samples are all white, therefore no absorption band is observed in the visible region of the spectra. In the UV region, all the as-synthesized samples show a broad band at about 220 – 320 nm (Fig. 7A), which arises from Al–O charge transfer transitions of framework and extra-framework tetrahedral $AlO_4$ species [37]. Similar absorption bands also appear in Fig. 7B for all the calcined samples of SAPO-34 and MgAPSO-34. This band is overlapped with a series of new bands at 225–270 nm for all the MgAPSO-34 samples. As shown in Fig. 7B for comparison, the absorbance of an MgO crystal [2] appears at
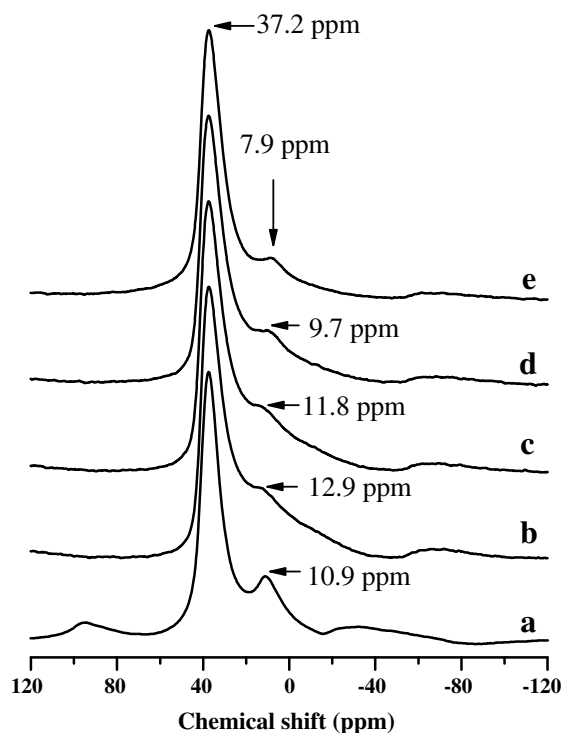
**Fig. 3.** $^{27}$Al MAS NMR spectra of as-synthesized samples. (a) Mg34-00, (b) Mg34-05, (c) Mg34-10, (d) Mg34-15 and (e) Mg34-20.
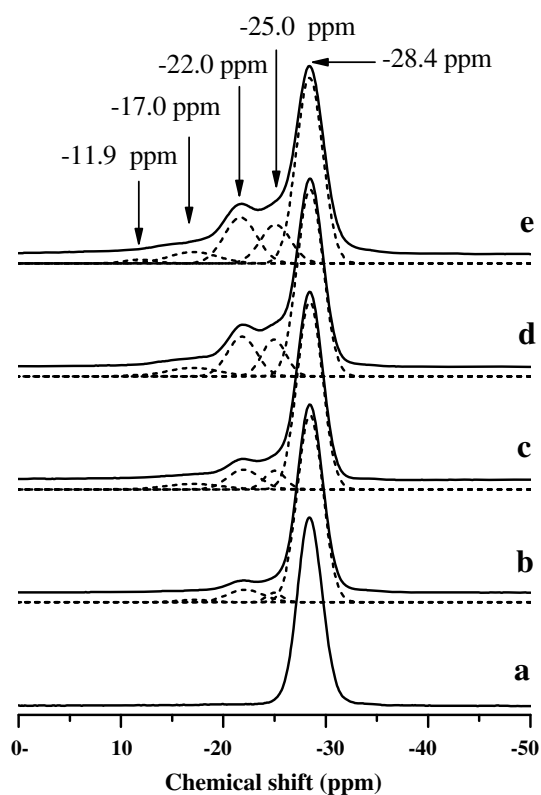
**Table 2**
The $^{31}$P MAS NMR results of the phosphorus percents in various co-ordination states

| Sample | Phosphorus co-ordination state (%) | | | |
|---|---|---|---|---|
| | P(4Al) | P(3Al, 1Mg) | P(2Al, 2Mg) | P(1Al, 3Mg) |
| | −28.4 ppm | −22.0, −25.0 ppm | −17.0 ppm | −11.9 ppm |
| Mg34-00 | 100.00 | 0.00 | 0.00 | 0.00 |
| Mg34-05 | 87.61 | 10.89 | 1.50 | 0.00 |
| Mg34-10 | 79.28 | 16.22 | 4.50 | 0.00 |
| Mg34-15 | 65.94 | 27.63 | 5.95 | 0.49 |
| Mg34-20 | 59.48 | 32.35 | 6.70 | 1.47 |



**Fig. 5.** $^{29}$Si MAS NMR spectra of as-synthesized samples. (a) Mg34-00, (b) Mg34-05, (c) Mg34-10, (d) Mg34-15 and (e) Mg34-20.
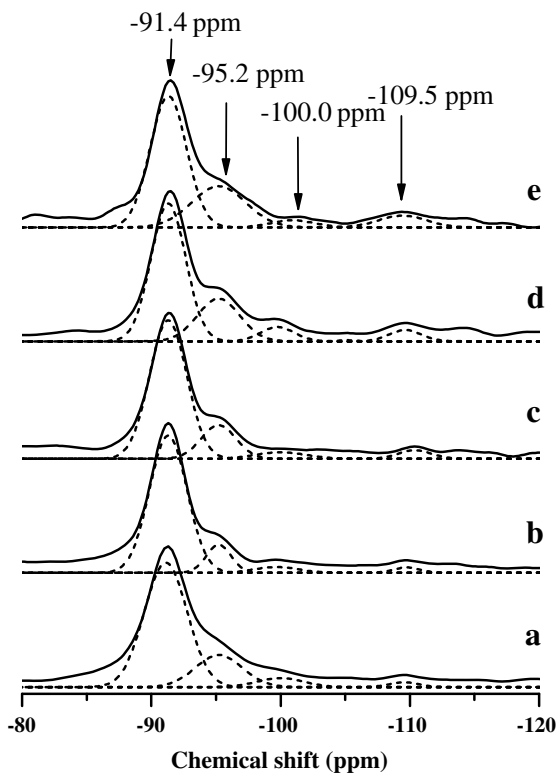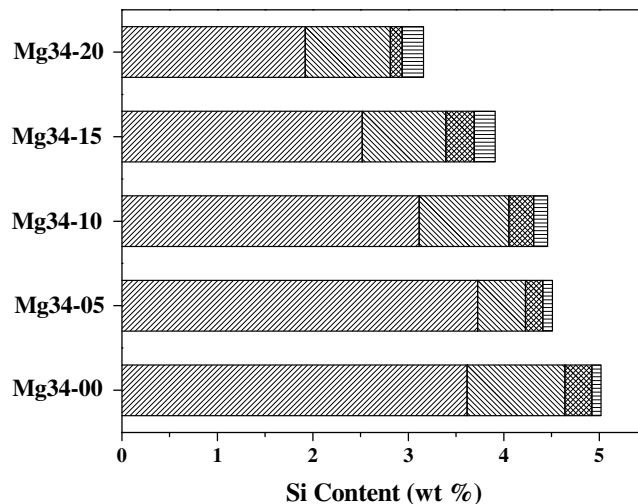


**Fig. 4.** $^{31}$P MAS NMR spectra of as-synthesized samples. (a) Mg34-00, (b) Mg34-05, (c) Mg34-10, (d) Mg34-15 and (e) Mg34-20.



**Fig. 6.** Silicon in various coordination environments from the $^{29}$Si MAS NMR spectra. Si(4Al), Si(3Al), Si(2Al), Si(0Al).

205 nm and an Mg-impregnated sample of Mg/SAPO-34 (Ref. [1]) gives the absorbance bands at 210–275 nm. This means that after
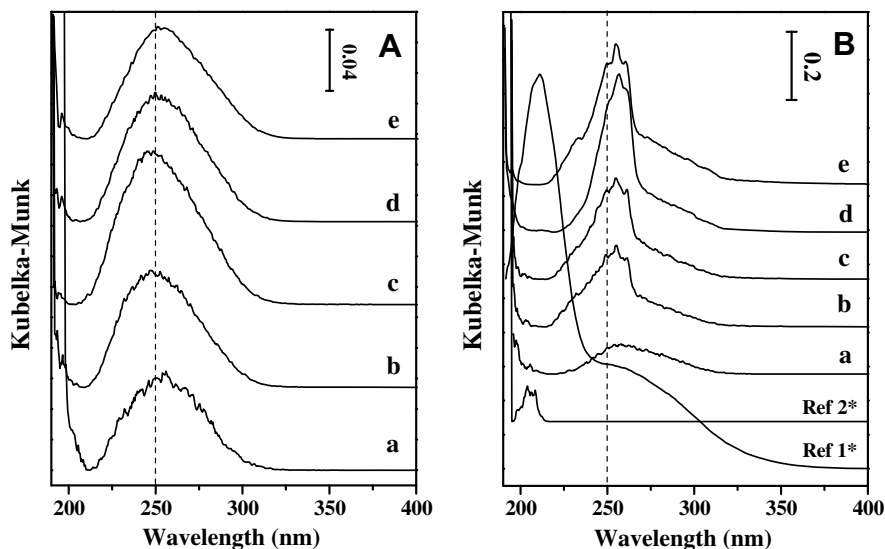
**Fig. 7.** UV–vis diffuse reflectance spectra of as-synthesized (A) and calcined (B) samples. (a) Mg34-00, (b) Mg34-05, (c) Mg34-10, (d) Mg34-15 and (e) Mg34-20. (*Ref [1], Mg/SAPO-34; Ref [2], MgO).

calcination, no Mg species from MgAPSO-34 transform into MgO and that all the Mg species are located in the framework, in accordance with the result obtained from XRD and $^{31}P$ MAS NMR. Hence the bands at 225–270 nm, present in the spectra of MgAPSO-34 overlapped with the broad band at 220–320 nm which are absent in spectra of SAPO-34 could be assigned to tetrahedral Mg species with 4- and 3-coordination. Their UV absorbencies are quite different from the absorbance of 4-coordination (225 nm) or 3-coordination (270 nm) within the MgO micro-crystal with unsaturated octahedral structure [38].

### 3.3. Acid measurement by NH$_3$-TPD and FT-IR

#### 3.3.1. Temperature programmed desorption of ammonia

Temperature programmed desorption of ammonia is used to determine the amount and strength of acid sites of the synthesized samples. The NH$_3$-TPD profiles of calcined SAPO-34 and MgAPSO-34 are shown in Fig. 8. The profiles consist of two distinct peaks, maxima at 170 – 190 °C and 350 – 416 °C, respectively. Due to the asymmetry of the second peak, these profiles could be deconvoluted into three clear desorption peaks (A, B and C), corresponding to the acid sites with differing strengths [35]. The results concerning the peak position and the amount of desorbed ammonia are presented in Table 3. Compared with SAPO-34, the amount of weak and moderate acid sites in MgAPSO-34 samples decreases with increasing Mg incorporation, while the amount of strong acid sites of Mg34-05 increases slightly. Further increase in Mg content within the frameworks gives rise to a gradual decrease in the number of acid sites. This may stem from less Si incorporation and the formation of more silica-islands in MgAPSO-34 samples with relatively high Mg content. As shown in Fig. 8 and Table 3, the general trend is that the total amount of acid sites decreases with increasing Mg content.

#### 3.3.2. FT-IR spectroscopy of NH$_3$ adsorption

Fig. 9A depicts the FT-IR spectra of the activated SAPO-34 and MgAPSO-34. The spectrum of Mg34-00 (Fig. 9A-a) shows two hydroxyl stretching vibration bands at 3625 and 3599 cm$^{-1}$, which are assigned to undisturbed bridged Si–OH–Al groups and bridged Si–OH–Al groups interacting with the oxygen atoms of the framework, respectively [39]. These two hydroxyl bands also appear in the spectra of Mg34-05 (Fig. 9A(b)) and Mg34-10 (Fig. 9A(c)), but
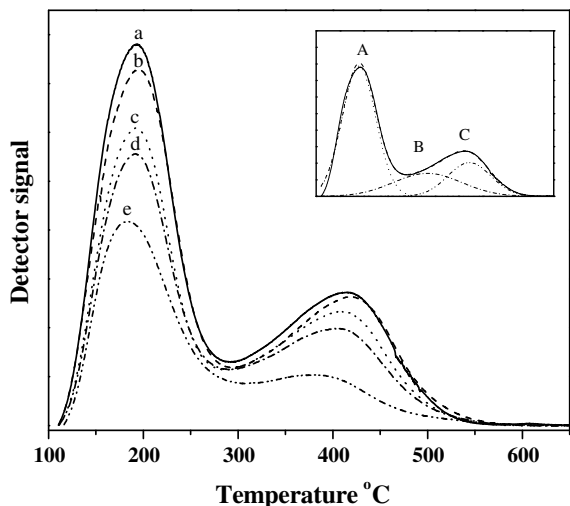


**Fig. 8.** NH$_3$-TPD profiles of SAPO-34 and MgAPSO-34s. (a) Mg34-00, (b) Mg34-05, (c) Mg34-10, (d) Mg34-15 and (e) Mg34-20.

**Table 3**
Acidity measurement with NH$_3$-TPD and FT-IR of NH$_3$ adsorption

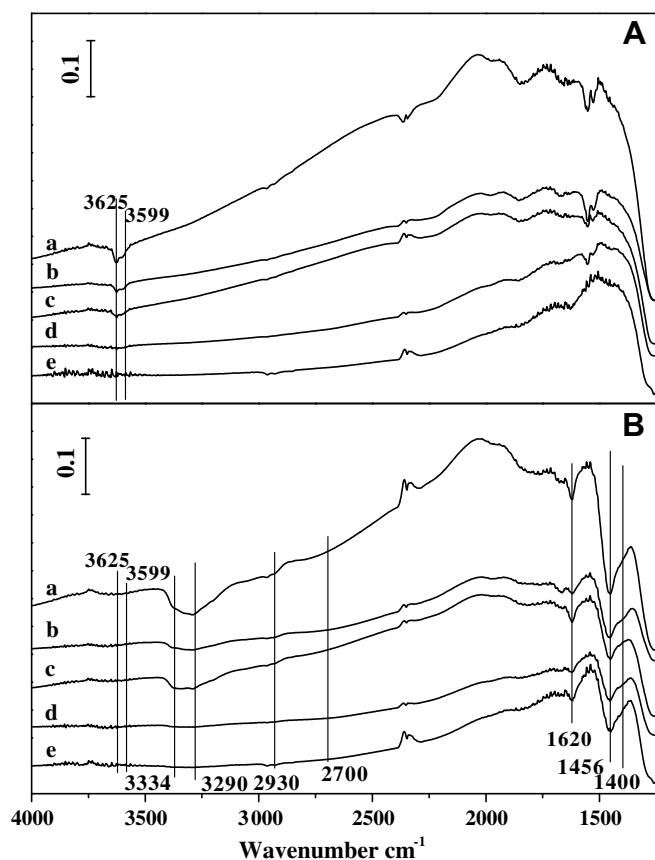| Sample | NH$_3$-TPD | | |
|---|---|---|---|
| | Acidity (NH$_3$ desorption (mmol/g)) | | |
| | Weak | Medium | Strong |
| | 182 – 192 °C | 315 – 334 °C | 410 – 422 °C |
| Mg34-00 | 0.2809 | 0.1006 | 0.0932 |
| Mg34-05 | 0.2752 | 0.0812 | 0.0980 |
| Mg34-10 | 0.2112 | 0.0892 | 0.0753 |
| Mg34-15 | 0.1906 | 0.0941 | 0.0584 |
| Mg34-20 | 0.1505 | 0.0590 | 0.0231 |

**Fig. 9.** Infrared spectra of activated samples (A) and NH$_3$-adsorbed samples (B). (a) Mg34-00, (b) Mg34-05, (c) Mg34-10, (d) Mg34-15 and (e) Mg34-20.

the intensity gradually decreases with Mg incorporation. In Mg34-15 and Mg34-20, these two bands almost disappear.

Upon adsorption of ammonia at 100 °C, the Si–OH–Al absorbance bands at 3625 and 3599 cm$^{-1}$ disappear and some new bands occur at 3400–1400 cm$^{-1}$ (Fig. 9B). The bands at 1456 and 1400 cm$^{-1}$ are usually assigned to the vibration of NH$_4^+$, generated by NH$_3$ adsorption on the Brönsted acid sites [40], while the band at 1620 cm$^{-1}$ is assigned to NH$_3$ adsorption on the Lewis acid sites. Compared with SAPO-34, SAPO-34 with Mg incorporation shows a decrease in the intensity of the bands arising from ammonia adsorption on Brönsted and Lewis acid sites at 1456, 1400 and 1620 cm$^{-1}$. These observations clearly demonstrate the surface acidity modification by Mg isomorphous substitution. The adsorption of ammonia also generates two other superimposed bands at 3334 and 3290 cm$^{-1}$ in the zone of 3000 and 3500 cm$^{-1}$, resulting from the interaction of ammonia with two types of hydroxyl groups at 3599 and 3625 cm$^{-1}$. It was previously reported that hydroxyl groups of zeolite or SAPO molecular sieves can be shifted to lower wave numbers upon the interaction with a molecular base [18,41–43]. No NH$_3$–OH interaction is present for Mg34-15 and Mg34-20 as no hydroxyls were detected by FT-IR.

### 3.4. Chloromethane conversion over SAPO-34 and MgAPSO-34

Catalytic transformation of chloromethane was carried out over SAPO-34 and MgAPSO-34. The evolution of conversion and product selectivity as a function of the time on stream is depicted in Fig. 10. The first analysis of the products made at time on stream of 5 min shows a very high conversion for all the tested catalysts, SAPO-34 and MgAPSO-34, indicating their high initial activity. All five catalysts gradually lose their activity with prolonged time on stream. It

is interesting to observe that for most of the Mg incorporated samples, the conversion loss is remarkably slower than that of Mg34-00, except for the Mg34-20 sample with the highest amount of Mg incorporated. This demonstrates that Mg incorporation into a SAPO-34 framework can be helpful in maintaining the catalytic activity of MgAPSO-34 catalysts. This improvement in catalyst life should be related to acidity modification by Mg incorporation, as discussion in Section 3.3.

A detailed product distribution given in Fig. 10 shows that product selectivity varies with the time on stream. At a reaction time of 5 min, high chloromethane conversion is observed with propane as the main product. Propylene and ethylene are also generated in relatively low selectivity. In prolonging the reaction time, light olefins become the main products. Ethylene selectivity increases gradually and attains more than 50% for all the catalysts studied. Propylene selectivity shows an increase at the time on stream of 35 min and remains constant at about 30% until 155 min in the following reaction period. Butene selectivity goes through a slight increase and then decrease slowly from 35 min time on stream. The variation in light olefin selectivity evolution could be the result of the modification of the catalyst pores by coke deposition during chloromethane transformation. With the production of a large amount of light olefins, alkane products, such as methane, ethane, propane, butane and products larger than C5 (C5$^+$) are produced with low selectivity. A mild increase in methane selectivity for longer reaction times may stem from the pore blockage by coke formation, favoring methane formation.

Comparing the catalytic properties of chloromethane transformation over SAPO-34 and MgAPSO-34, Mg incorporation gives rise to a remarkable increase in catalyst life. Mg incorporation also affected the light olefin selectivity. SAPO-34 shows a relatively higher selectivity for ethylene production. Propylene generation is more predominate over MgAPSO-34 than SAPO-34.

The general reaction path of the conversion of chloromethane into hydrocarbons is described in Scheme 1 [4,28,30].

Light olefins have been proposed to be the initial products of chloromethane transformation over an acid catalyst [16,19]. The final light olefin selectivity is closely related to the secondary reactions, such as oligomerization, H-transfer reactions and cracking. A useful parameter, the Hydrogen Transfer Index (HTI, C$_3^o$/C$_3^=$), is employed to measure the hydrogen transfer level of SAPO-34 and MgAPSO-34 catalysts [44]. Fig. 11 gives the HTI value of chloromethane conversion over SAPO-34 and MgAPSO-34. For all the catalysts, a high conversion is accompanied by a high HTI value, corresponding to high propane selectivity and low propylene selectivity during the initial reaction stage. In prolonging the reaction time, the HTI value is lowered with a decrease in conversion. Light olefins become the main products in chloromethane transformation. A detailed comparison shows that at the same level of chloromethane conversion, Mg34-05 has the lowest HTI value. The hydrogen transfer reaction could be weakened by using Mg-incorporated SAPO-34 catalysts.

Pore structure and acidity affect the hydrogen transfer level. A large void space and a high density of Brönsted acid sites, especially the acid sites in the neighborhood, are very important for hydrogen transfer reactions [44–47]. For SAPO-34 and MgAPSO-34, which have very similar pore structures, the HTI values would be mainly influenced by their acid strength and density. As shown by FT-IR and NH$_3$-TPD in Section 3.3, the presence of Mg induces the reduction of Si substitution into the AlPO framework and thus less acid site formation. This weakened acidity with Mg incorporation is responsible for the lowered HTI value and the improved light olefin selectivity. The total ethylene and propylene selectivity reaches 80% over MgAPSO-34, indicating that MgAPSO-34 is a potential catalyst for light olefin production.
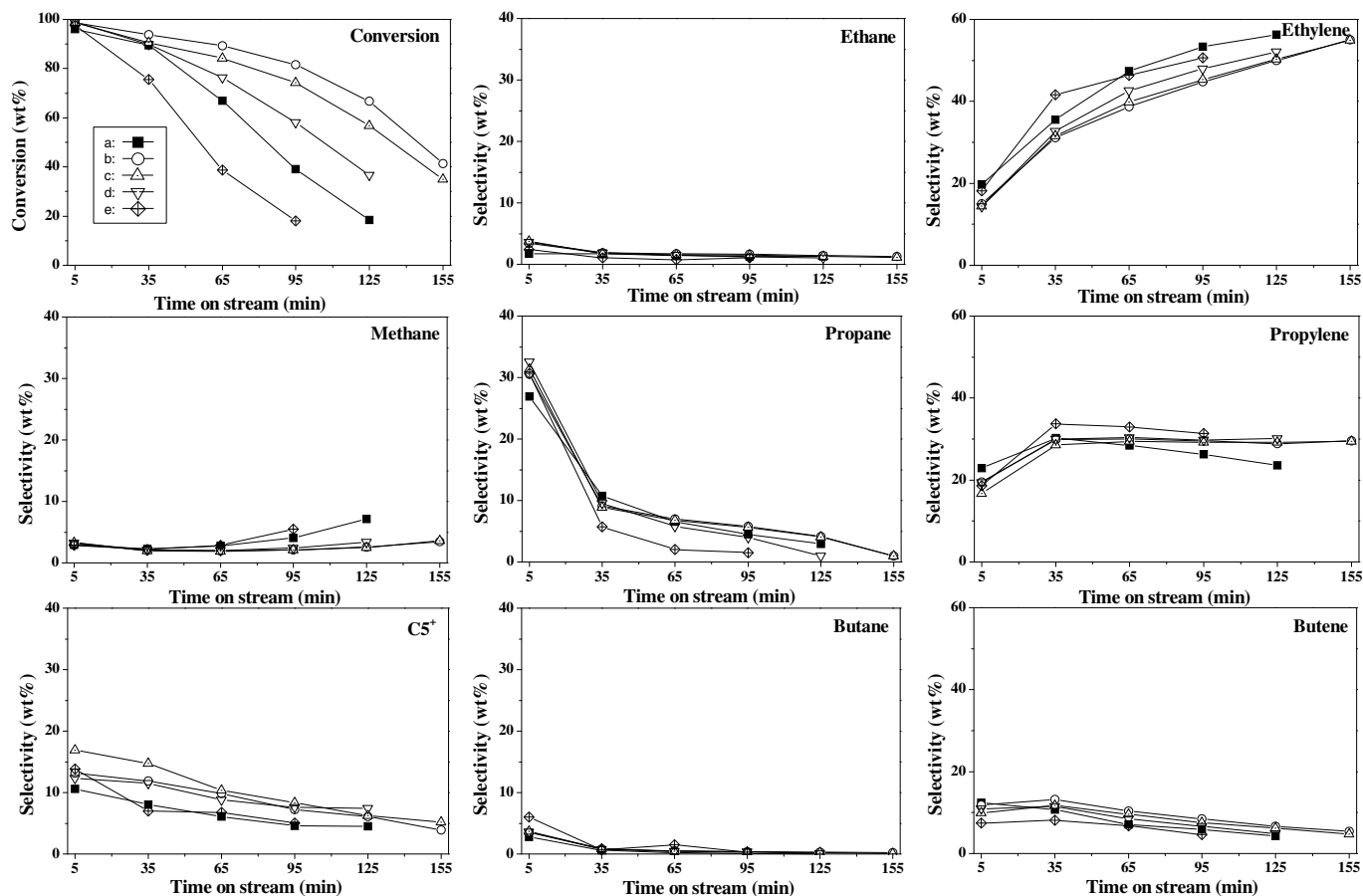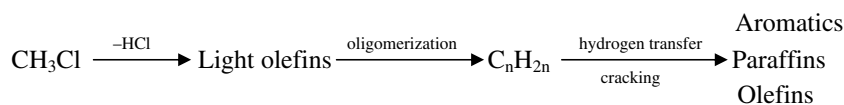
**Fig. 10.** The conversion and selectivity of chloromethane reaction over SAPO-34 and MgAPSO-34 catalysts ($T$ = 450 °C, WHSV = 3.17 h$^{-1}$). (a) Mg34-00, (b) Mg34-05, (c) Mg34-10, (d) Mg34-15 and (e) Mg34-20.

$$CH_3Cl \xrightarrow{-HCl} \text{Light olefins} \xrightarrow{\text{oligomerization}} C_nH_{2n} \xrightarrow[\text{cracking}]{\text{hydrogen transfer}} \begin{array}{l} \text{Aromatics} \\ \text{Paraffins} \\ \text{Olefins} \end{array}$$
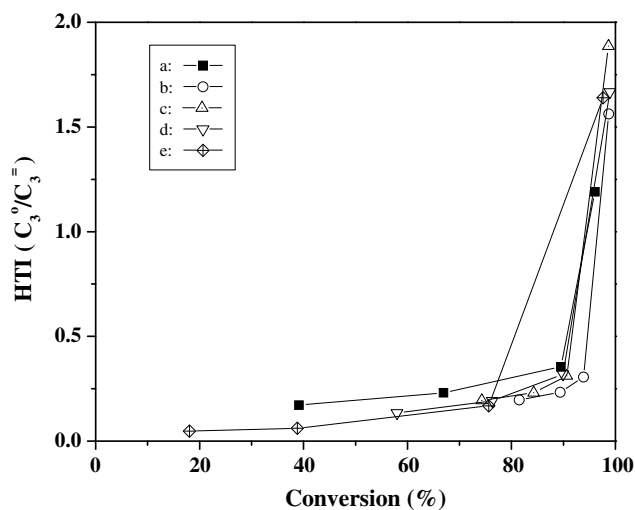
**Scheme 1.**



**Fig. 11.** Conversion vs. HTI (Hydrogen Transfer Index) plots of chloromethane transformation over SAPO-34 and MgAPSO-34 catalysts. (a) Mg34-00, (b) Mg34-05, (c) Mg34-10, (d) Mg34-15 and (e) Mg34-20.

## 4. Conclusions

SAPO-34 and MgAPSO-34 with a CHA zeolite structure were synthesized for applications in light olefin production from chloromethane transformation. Mg incorporation into SAPO-34 molecular sieves gave rise to the differences in crystalline structure, morphology, P and Si chemical environments and acidity. The increase in unit cell parameter and particle size was observed for Mg containing samples. The appearance of new tetrahedral P and Mg species in $^{31}$P MAS NMR and UV–vis spectra proved that Mg is substituted for Al within the SAPO framework. The presence of Mg in the starting synthesis gel reduced the Si incorporation and induced Si chemical environments of MgAPSO-34. NH$_3$-TPD and FT-IR results showed relatively weak acidity and less acid sites for Mg-incorporated samples. Catalytic performance tests showed that both SAPO-34 and MgAPSO-34 molecular sieves were very active and selective catalysts for the production of light olefins via chloromethane transformation. Mg modification could efficiently lower the hydrogen transfer reaction level and contribute to the improved catalyst life and light olefin selectivity, in particular for propylene production.

## References

[1] S. Wilson, P. Barger, Micropor. Mesopor. Mater. 29 (1999) 117.
[2] S. Hocevar, J. Levec, J. Catal. 135 (1992) 518.
[3] D.B. Akolekar, J. Mol. Catal. A: Chem. 104 (1995) 95.
[4] M. Stoecker, Micropor. Mesopor. Mater. 29 (1999) 3.
[5] M. Hartmann, L. Kevan, Chem. Rev. 99 (1999) 635.
[6] B.M. Weckhuysen, R.R. Rao, J.A. Martens, R.A. Schoonheydt, Eur. J. Inorg. Chem. (1999) 565.
[7] T. Inui, M. Kang, Appl. Catal. A-Gen. 164 (1997) 211.
[8] H. Sun, S.N. Vaughn, US6040264, 2000.
[9] W.L. Shea, R.B. Borade, A. Clearfield, J. Chem. Soc. Faraday Trans. 89 (1993) 3143.
[10] J.J. Li, Y. Guo, G.D. Li, J.S. Chen, C.J. Li, Y.C. Zou, Micropor. Mesopor. Mater. 79 (2005) 79.
[11] F. Deng, Y. Yue, T.C. Xiao, Y.U. Du, C.H. Ye, L.D. An, H.L. Wang, J. Phys. Chem. 99 (1995) 6029.
[12] S. Ashtekar, A.M. Prakash, D.K. Chakrabarty, S.V.V. Chilukuri, J. Chem. Soc. Faraday Trans. 92 (1996) 2481.
[13] D.E. Akporiaye, A. Andersen, I.M. Dahl, H.B. Mostad, R. Wendelbo, J. Phys. Chem. 99 (1995) 14142.
[14] M. Kang, J. Mol. Catal. A: Chem. 160 (2000) 437.
[15] D.R. Dubois, D.L. Obrzut, J. Liu, J. Thundimadathil, P.M. Adekkanattu, J.A. Guin, A. Punnoose, M.S. Seehra, Fuel Process. Technol. 83 (2003) 203.
[16] Y.X. Wei, D.Z. Zhang, Z.M. Liu, B.L. Su, J. Catal. 238 (2006) 46.
[17] Y.X. Wei, D.Z. Zhang, L. Xu, Z.M. Liu, B.L. Su, Catal. Today 106 (2005) 84.
[18] Y.X. Wei, Y.L. He, D.Z. Zhang, L. Xu, S.H. Meng, Z.M. Liu, B.L. Su, Micropor. Mesopor. Mater. 90 (2006) 188.
[19] D.Z. Zhang, Y.X. Wei, L. Xu, A.P. Du, F.X. Chang, B.L. Su, Z.M. Liu, Catal. Lett. 109 (2006) 97.
[20] Y.X. Wei, D.Z. Zhang, Z.M. Liu, B.L. Su, Chem. Phys. Lett. 4444 (2007) 197.
[21] Y.X. Wei, D.Z. Zhang, L. Xu, F.X. Chang, Y.L. He, S.H. Meng, B.L. Su, Z.M. Liu, Catal. Today 131 (2008) 262.
[22] S. Svelle, S. Arwinthan, M. Bjorgen, K.P. Lillerud, S. Kolboe, I.M. Dahl, U. Olsbye, J. Catal. 241 (2006) 243.
[23] G.A. Olah, B. Gupta, M. Farina, J.D. Felberg, W.M. Ip, A. Husain, R. Karpeles, K. Lammertsma, A.K. Melhotra, N.J. Trivedi, J. Am. Chem. Soc. 107 (1985) 7097.
[24] C.E. Taylor, R.P. Noceti, R.R. Schehl, in: D.M. Bibby, C.D. Chang, R.F. Howe, S. Yurchak (Eds.), Methane conversion, Stud. Surf. Sci. Catal. Elsevier, Amsterdam, 36, 1988, 483.
[25] C.E. Taylor, in: A. Corma, F.V. Melo, S. Mendioroz, J.L.G. Fierro (Eds.), 12th International Congress on Catalysis, Stud. Surf. Sci. Catal. Elsevier, Amsterdam, 130, 2000, 3633.
[26] P. Lersch, F. Bandermann, Appl. Catal. 75 (1991) 133.
[27] Y. Sun, S.M. Campbell, J.H. Lunsford, G.E. Lewis, D. Palke, L.M. Tau, J. Catal. 143 (1993) 32.
[28] S. Svelle, S. Kolboe, U. Olsbye, O. Swang, J. Phys. Chem. B 107 (2003) 5251.
[29] D. Jaumain, B.L. Su, in: A. Corma, F.V. Melo, S. Mendioroz, J.L.G. Fierro (Eds.), 12th International Congress on Catalysis, Stud. Surf. Sci. Catal. Elsevier, Amsterdam, 130, 2000, 1607.
[30] D. Jaumain, B.L. Su, J. Mol. Catal. A: Chem. 197 (2003) 263.
[31] D. Jaumain, B.L. Su, Catal. Today 73 (2002) 187.
[32] X.R. Xia, Y.L. Bi, T.H. Wu, K.J. Zhen, Catal. Lett. 33 (1995) 75.
[33] J. Tan, Z.M. Liu, X.H. Bao, X.C. Liu, X.W. Han, C.Q. He, R.S. Zhai, Micropor. Mesopor. Mater. 53 (2002) 97.
[34] C.S. Blackwell, R.L. Patton, J. Phys. Chem. 92 (1988) 3965.
[35] S. Ashtekar, S.V.V. Chilukuri, D.K. Chakrabarty, J. Phys. Chem. 98 (1994) 4878.
[36] D. Barthomeuf, Zeolites 14 (1994) 394.
[37] M.A. Zanjanchi, A. Ghanadzadeh, F. Khadem-Nahvi, J. Inclusion Phenom. Mol. Recognit. Chem. 42 (2002) 295.
[38] M. Sterrer, T. Berger, O. Diwald, E. Knoezinger, J. Am. Chem. Soc. 125 (2003) 195.
[39] S.A. Zubkov, L.M. Kustov, V.B. Kazansky, I. Girnus, R. Fricke, J. Chem. Soc. Faraday Trans. 87 (1991) 897.
[40] R. Vomscheid, M. Briend, M.J. Peltre, D. Barthomeuf, P.P. Man, J. Chem. Soc. Faraday Trans. 91 (1995) 3281.
[41] B.L. Su, D. Barthomeuf, J. Catal. 139 (1993) 81.
[42] V. Norberg, B.L. Su, Zeolites 19 (1997) 65.
[43] B.L. Su, D. Barthomeuf, J. Chem. Soc. Faraday Trans. 89 (1993) 857.
[44] A. Corma, V. Gonzalez-Alfaro, A.V. Orchilles, Appl. Catal. A-Gen. 187 (1999) 245.
[45] M.A. Sanchez-Castillo, R.J. Madon, J.A. Dumesic, J. Phys. Chem. B 109 (2005) 2164.
[46] G. de la Puente, E.F. Sousa-Aguiar, A.F. Costa, U. Sedran, Appl. Catal. A-Gen. 242 (2003) 381.
[47] A. Martinez, C. Lopez, Appl. Catal. A-Gen. 294 (2005) 251.